Near to Long-Wave Infrared Mercury Chalcogenide Nanocrystals from Liquid Mercury

Nicolas Goubet, Maxime Thomas, Charlie Gréboval, Audrey Chu, Junling Qu, Prachi Rastogi, Sang-Soo Chee, Mayank Goyal, Yimin Zhang, Xiang Zhen Xu, et al.

Near to Long-Wave Infrared Mercury Chalcogenide Nanocrystals from Liquid Mercury

Nicolas Goubet[1,2,3*], Maxime Thomas[2], Charlie Gréboval[1], Audrey Chu[1], Junling Qu[1], Prachi Rastogi[1], Sang-Soo Chee[1], Mayank Goyal[1], Yimin Zhang[1], Xiang Zhen Xu[2], Gregory Cabailh[1], Sandrine Ithurria[2], Emmanuel Lhuillier[1*]

[1] Sorbonne Université, CNRS, Institut des NanoSciences de Paris, 4 place Jussieu, 75005 Paris, France.

[2] Laboratoire de Physique et d'Etude des Matériaux, ESPCI-Paris, PSL Research University, Sorbonne Université Univ Paris 06, CNRS UMR 8213, 10 rue Vauquelin, 75005 Paris, France.

[3] Sorbonne Université, CNRS, Monaris, 4 place Jussieu, 75005 Paris, France.

ABSTRACT: HgTe nanocrystals are currently the most promising colloidal material for infrared detection, combining broadly tunable infrared absorption and photoconductive properties. Current synthesis leads to a limited amount of material and relies on a highly toxic water-soluble form of Hg. Here, we explore the possibility of using Hg thiolate as Hg source and demonstrate that the latter can be formed *in situ* from liquid Hg. The developed protocol allows large masses (7 g) and highly concentrated (100 g/L) synthesis, which is a step forward for the transfer of this material towards industry. The transport properties of the material have also been investigated and we observe a transition from p to n-type with size. We observe that the threshold of the p to n switch depends on the growth method which enables for a given size of nanocrystal the formation of p-n junction. This work has great potential to design infrared sensor with optimized charge dissociation.

INTRODUCTION

The ease for tuning the spectrum of colloidal quantum dots (CQDs) from UV to the THz range[1] is certainly one of their most striking properties. While in the visible range their emitting properties have been used for applications such as displays and light emitting diodes[2], in the infrared range[3], it is rather their absorption and photoconductive features which are valuable to design solar cells[4–6] and infrared sensors.[7–9] In the near infrared, PbS and PbSe[10] CQDs have reached a high level of maturity with polydispersity down to 3%. This corresponds to a size fluctuation of a single monolayer.[11] When longer infrared wavelengths (λ>2 µm) are concerned, HgTe has led to the best photoconductive properties[12–15] and promising light emission[16,17] in the mid-infrared or lasing[18] in the short-wave infrared.

When it comes to synthesizing nanocrystals (NCs) absorbing above 3 µm, which is critical for thermal imaging applications, the number of available synthesis methodologies becomes limited.[19–21] Kovalenko *et al*[21] proposed a synthesis based on the *in situ* formation of HgTe in aqueous medium to overcome the difficulty of handling a gaseous precursor. However, the material was limited to wavelengths below 3.5 µm. Later, Keuleyan *et al*[22,23] developed an organic approach using $HgCl_2$ dissolved in oleylamine that reacts with Te complexed with trioctylphosphine (TOP:Te). The same group then improved the size distribution and shape control by replacing the TOP:Te by bis(trimethylsilyl)telluride, which does not go in the direction of reduced toxicity or easier handling.[24] Indeed, most of the previous literature on HgTe synthesis has focused on the use of mercury salts, where Hg is in the Hg^{+II} state, which is extremely soluble in water. In addition, the material quality and, in particular the size distribution is strongly improved by diluting the reaction medium.[23] As a result, current syntheses are conducted in diluted conditions and this is a key limitation to scale-up the HgTe NCs synthesis. It was recently demonstrated that the workforce is the main cost relative to nanocrystal synthesis.[25] In this sense, dilute processes require more syntheses to obtain the same amount of material and further increase workforce exposure to heavy metals. Developing new path which allow concentrated synthesis of HgTe while preserving the spectral tunability in the infrared appears of utmost interest.

In this paper, we develop a new synthetic method for the synthesis of mercury chalcogenide CQDs based on liquid mercury as Hg source. Liquid Hg does not appear as a common mercury source for colloidal synthesis, whereas it has been widely used in the case of liquid phase epitaxy as employed for the growth of bulk HgCdTe and HgTe based heterostructures. In addition, to reduce the toxicity of the mercury precursor, this procedure allows to achieve extremely concentrated syntheses (up to 400 mM [Hg]). The procedure is used to produce up to 7 g of material from a single synthesis carried out in conventional laboratory conditions (*i.e.* from a 100 mL total volume). In addition, the procedure leads to broadly tunable absorption from 1000 to 10000 cm^{-1}. Last, we demonstrate that the doping magnitude of the material can be controlled by the choice of the growth procedure, enabling the formation of p-n junction made of only one nanocrystal size.

EXPERIMENTAL SECTION

Nanocrystal synthesis

Chemicals : Te powder 30 mesh (Alfa Aesar, 99.99%), Se powder (Sigma-Aldrich, 99,99%), sulfur powder (Sigma Aldrich, 99,99%), bis(trimethylsilyl) sulfide (Sigma-Aldrich), $(NH_4)_2S$ (Sigma Aldrich, 20 wt. % in H_2O), mercury acetate (Sigma-Aldrich, ≥98%), mercury chloride (Sigma-Aldrich, ≥99,5%), mercury bromide (Strem Chemicals), mercury iodide (Strem Chemicals, 99%), iodine (Sigma-Aldrich, 99.99%), Trioctylphosphine (TOP, Cytek, 90%), dodecanethiol (DDT, Sigma Aldrich), ethanedithiol (EDT, Sigma-Aldrich, ≥98%), oleylamine (Acros, 80-90%), ethanol (VWR, ≥99.8%), methanol (VWR, ≥99.8%), toluene (VWR, ≥99.8%), lithium perchlorate (Sigma-Aldrich, 98%), polyethylene glycol (MW = 6 kg mol^{-1}), the water used was purified with a Milipore system (18.2 MΩ).

TOP:Te precursor (1 M) : 2.54 g of Te powder are mixed in 20 mL of TOP in a three-neck flask. The flask is kept under vacuum at room temperature for 1 hour. The atmosphere is then switched to Ar and the temperature is raised to 275 °C. The solution is stirred until a clear orange solution is obtained. The flask is then cooled down and the color switches to yellow. At room temperature, the flask is degassed again for 10 min. Finally, this solution is transferred to a glove box for storage.

Mercury thiolate precursor: 3.18 g of mercury acetate are dissolved in 150 mL of water. The mercury solution is then added to a solution of 5 mL of dodecanethiol in 250 mL of ethanol. Mercury dodecylthiolate is precipitated immediately in white powder. After decanting, the solid product is filtered and washed several times with ethanol (150 mL). The white powder is dried and recrystallized in hot toluene.

Synthesis of HgTe nanocrystal from Hg thiolate: 0.6 g of mercury dodecylthiolate is dissolved in 4 mL of oleylamine and degassed at 100 °C for 10 min. Under Ar atmosphere, 1 mL of TOP:Te (1M) is injected to the thiolate solution at the desired temperature. The solution immediately turns from colorless to black-brown color. After 1 min, 1 mL of dodecanethiol is injected to quench the reaction. Nanocrystals are precipitated with 10 mL of methanol. After precipitation, the nanocrystals are redispersed with 2 mL of chloroform and few drops of dodecanethiol. The previous two steps are repeated twice with 5 mL of methanol. Finally, nanocrystals are redispersed in chloroform.

Synthesis from liquid mercury: 0.2 g of liquid mercury is sonicated in 2 mL of dodecanethiol during 15 min. The solution turn from colorless to a metallic grey color. 2 mL of oleylamine and 26 mg of iodine are added to the mercury solution and degassed at room temperature for 15 min. Slight discoloration is observed during the degassing step. Under argon atmosphere, 1 mL of TOP:Te (1 M) is injected to the mercury solution at the desired temperature. The solution color turns from grey to a black-brown solution. After 1 min, 1 mL of dodecanethiol is injected to quench the reaction. Nanocrystals are precipitated with 10 mL of methanol. After precipitation, the nanocrystals are redispersed with 2 mL of chloroform and few drops of dodecanethiol. The precipitation step is repeated with 5 mL of methanol. Finally, nanocrystals are redispersed in chloroform.

Large scale synthesis from liquid mercury In a 250 mL three-neck flask, 8 g of liquid mercury is sonicated in 30 mL of dodecanethiol for 8 hours. After adding 1.04 g of iodine and 30 mL of oleylamine, the mercury solution is degassed at room temperature for 30 min. The atmosphere is flushed with Ar and placed again under vacuum. At 90 °C, 40 mL of TOP:Te (1 M) is injected under vacuum to increase the injection speed[26] and the reaction is conducted for 3 min. The reaction is quenched by adding 20 mL of dodecanethiol. The temperature decreases with ice bath to room temperature. Nanocrystals are precipitated with 40 mL of methanol. After precipitation, the nanocrystals are redispersed with 20 mL of chloroform and few drops of dodecanethiol. The precipitation step is repeated with 10 mL of methanol. Finally, nanocrystals are redispersed in chloroform. In summary, only 100 mL of reaction medium and 50 mL of cleaning solvent are necessary to obtain ≈7 g of short wave infrared active nanomaterials.

Material characterization

Optical spectroscopy: Absorption spectra are acquired using a Shimadzu 3600 spectrometer for the UV visible part, while a Thermo Fischer IS50 Fourrier transform infrared spectrometer in ATR configuration for the near infrared and a Bruker Vertex 70 for the mid infrared are used.

Microscopy: For transmission electron microscopy, we used a JEOL 2010. The grids were prepared by a drop-cast of diluted solution of nanocrystals dispersed in hexane and degassed overnight under secondary vacuum.

Diffraction: X-ray diffraction pattern is obtained by drop-casting the solution of nanocrystals on a Si wafer. The diffractometer is a Philips X'Pert, based on the emission of the Cu Kα line operated at 40 kV and 40 mA current.

Elemental analysis using X-ray dispersive spectroscopy (EDX): For EDX analysis the particles are spread on a conductive carbon tape. The EDX analysis is performed by a FEI Magellan scanning electron microscope operated at 15 kV and 1.6 nA. The X-ray analysis is made with an Oxford probe.

Photoemission spectroscopy: 80 nm-thick gold is evaporated on a Si wafer and used as conductive substrate. The film of nanoparticles is deposited, and the pristine ligands are exchanged with ethanedithiol. The film is then introduced to the preparation chamber and then degassed until a vacuum in the 10^{-10} mbar range is reached. The sample is finally loaded into the analysis chamber. During the XPS measurements, the photoelectrons are detected at normal emission from the polarization vector $\vec{E}$. A photon energy of 1486.7 eV (Al K_α) was used. For the photoelectrons analysis we used 50 eV pass energy. To calibrate the system, we shift the data to set the energy of the C 1s core level equal to 284.8 eV. This shift is applied to all other spectra to get the actual kinetic energy value. Then all spectra are plotted as a function of binding energy following the formula BE = 1486.7 – cKE, where cKE is the corrected kinetic energy.

Transport measurements

Electrode fabrication: The surface of a Si/SiO_2 wafer (400 nm oxide layer) is cleaned by sonication in acetone. The wafer is rinsed with isopropanol and finally cleaned using an O_2 plasma. AZ 5214E resist is spin-coated and baked at 110 °C for 90 s. The substrate is exposed under UV through a pattern mask for 2 s. The film is further baked at 125 °C for 2 min to invert the resist. Then a 40 s flood exposure is performed. The resist is developed using a bath of AZ 726 for 32 s, before being rinsed in pure water. We then deposit a 5 nm chromium layer and 80 nm gold layer using a thermal evaporator. The lift-off is performed by dipping the film in acetone for 1 hour. The electrodes are finally rinsed using isopropanol and dried by an air flow. The electrodes are 2.5 mm long and spaced by 20 µm.

Electrolyte preparation: For electrolyte gating, we first mixed 0.5 g of $LiClO_4$ with 2.3 g of PEG (M_W = 6 $kg.mol^{-1}$) in a glove box. The solution is heated at 170 °C on a hot plate for 2 hours until the solution gets clear. To use the electrolyte, the solution is warmed around 80 °C and brushed on the top of the HgTe nanoparticle film.

Thin film deposition and ligand exchange: Ligand exchange is performed on solid-state film. The HgTe QDs film is prepared by drop-cast of a colloidal solution in chloroform on 20 µm spaced electrodes. The film is dipped in a 1-2 vol% EDT/ethanol solution for 1 min. Ethanol is used to rinse the film after each HgTe QD deposition and EDT ligand exchange cycle. A drop of viscous electrolyte is deposited on the nanocrystal film. After PEG solidification, the device is dried overnight under vacuum.

Transistor characterization: The sample is connected to two Keithley 2400. The first, sets the drain bias (50 mV < V_{DS} < 500 mV) and measures the associated drain current. The second, tunes the gate bias (V_{GS}) between -2 and +2 V with a step of 1 mV and measures the associated gate current. All measurements are conducted under room conditions (temperature and pressure). A scheme of the device is given in Figure S18.

DISCUSSION

Current syntheses of mid-infrared HgTe NCs particularly suffer from the low solubility of $HgCl_2$ in amines which are commonly used as coordinating solvent. Thus organo-soluble precursors of mercury are of utmost interest. Here we take advantage of the strong affinity of Hg for sulfur to prepare mercury thiolate as the Hg source.[27] The latter is prepared by the reaction of Hg^{2+} salt with dodecanethiol (DDT). DDT has been previously introduced in HgTe syntheses, however, the purpose was to slow down the reaction to grow small NCs.[18,28] The obtained mercury dodecylthiolate precursor is a white powder, see Figure 1a, with a lamellar crystalline structure according to X-ray diffraction and scanning electron microscopy (SEM), see Figure 1a and S1. The reaction to synthesize HgTe nanocrystals (Figure 1b) is conducted using trioctylphosphine telluride (TOP:Te) as Te source in presence of oleylamine. The amine is critical to obtain non-aggregated NCs with a sharp band edge transition, see Figure S2.

Figure 1c displays the infrared spectrum of the obtained nanoparticles with various sizes obtained for different temperatures of synthesis. There are three main contributions in the spectra of these nanoparticles. (*i*) At large wavenumber (*ie* high energy) there is a broad band absorption relative to interband transitions (*ie* transition from valance band to conduction band). By tuning the reaction temperature from 50 to 180 °C the interband-edge energy can be tuned from 10000 cm^{-1} to 2000 cm^{-1}

(equivalent to the range between 1.2 eV and 250 meV), see Figure S3, S14 and Figure 1c. (*ii*) At low wavenumber below 1000 cm^{-1} (ie low energy part of the spectrum) there is a peak relative to intraband transition.[24] This peak is only observed for the largest nanoparticles. This absorption is the result of self-doping,[29,30] which is a very specific doping mechanism of narrow band gap nanocrystal.[31] Because of their narrow band gap nature and because of their small non-stoichiometry (energy dispersive X-ray spectroscopy reveals an Hg excess, see table S1) the Fermi level can be above the conduction band leading to degenerate doping. In HgTe, this process only occurs when the band gap is narrow enough,[1,24] as a result only the largest nanoparticles present this behavior. (*iii*) Last, the spectrum presents some sharp lines resulting from organic and this is mostly associated with the capping ligands. Here dodecanethiol is the main grafted molecule and we observe clear signatures for C-H bond stretch (2924 cm^{-1}), C-H bond bending (1466 cm^{-1}), C-S bond at 725 cm^{-1}. CO_2 contribution at 2340 cm^{-1} may also appear due to the fact that measurements are conducted in air.

Because HgTe is a semimetal (*i.e.* zero band gap semiconductor) and has a large Bohr radius[32,33] (≈40 nm), we can directly attribute the observed spectral tunability to quantum confinement: NCs size is tuned from 3 to 25 nm with the synthesis, see Figure 1b and Figure S4. Obtained NCs have a zinc blende lattice (Figure S5) and are cation-rich according to energy dispersive X-ray spectroscopy, see Table S1.

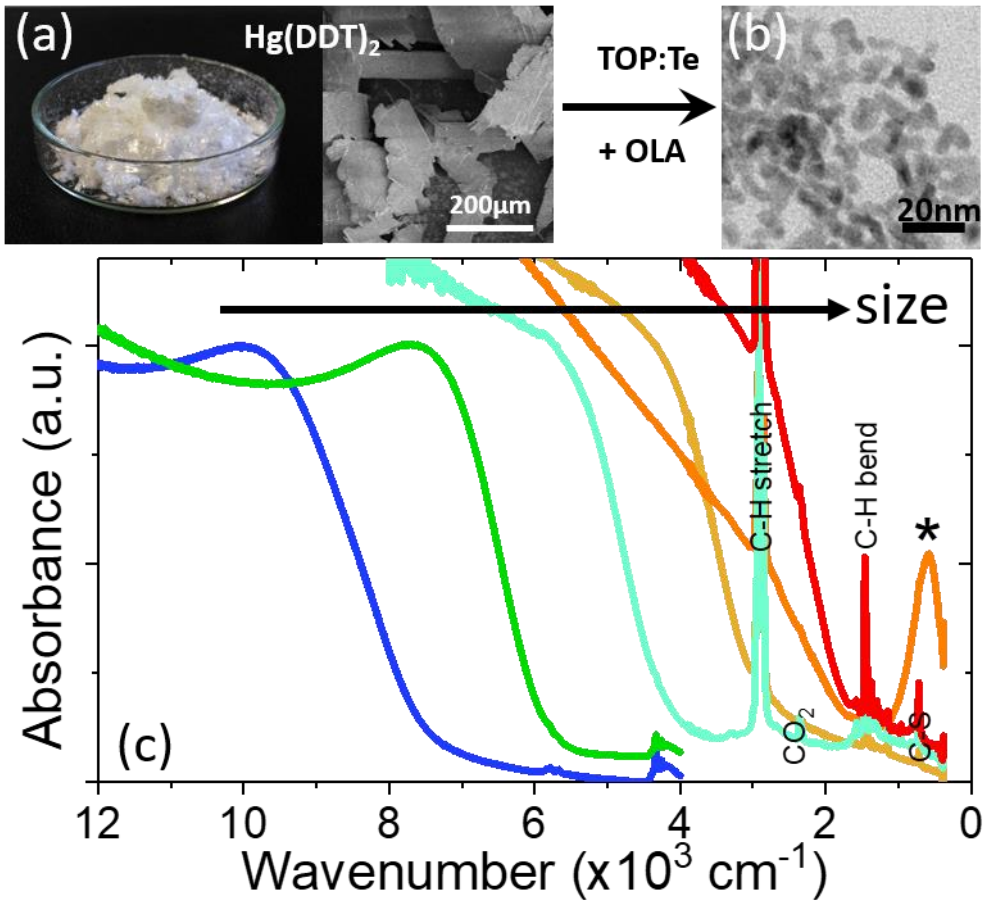

*Figure 1 (a) Optical and scanning electron microscopy SEM pictures of mercury dodecylthiolate ($Hg(DDT_2)$) and its use to grow HgTe NCs. (b) TEM pictures of HgTe QDs synthesized with $Hg(DDT_2)$ at 150 °C. (c) Absorbance spectra of HgTe QDs synthesized from 50 °C (blue) to 200 °C (orange) using $Hg(DDT_2)$ as Hg precursor. * is here to highlight the intraband contribution of the absorption spectrum.*

While mercury thiolate appears as a promising route, we aim to use this strategy to reduce the toxicity of the protocol. Commonly used Hg^{2+} salts are strongly water (and then blood) soluble, which is not the case of liquid mercury.[34] In the following, we propose a synthetic procedure where the mercury thiolate is prepared *in situ* from liquid mercury. We sonicate liquid Hg in DDT for several hours[35] and then obtain a mixture of mercury thiolate crystals and colloidal liquid Hg,[36] see Figure 2a and b and Figure S7.

If the reaction toward HgTe NCs is conducted from this mixture, we collect a significant amount of colloidally unstable material. The reaction leads to the formation of a HgTe nanorod array, see Figure S8 and S9. The addition of iodine[37] in the reaction medium favours the formation of the stable fraction, see Figure S10. In this case, iodine is expected to behave as an oxidizing agent for Hg^0 toward Hg^{2+}.[37] This method allows a broad tuning of the band-edge energy from 8000 to 1000 cm^{-1} for interband transitions and up to 500 cm^{-1} for intraband transitions, see Figure 2d and S11. The obtained NCs have a non-spherical shape, see Figure 2c and S12.

There are two important details that remain to be revealed about this procedure, including the crystallinity and the actual redox state of Hg. We confirm that obtained nanoparticles are crystalline with a zinc-blende atomic lattice (Figure 2f). It is worth mentioning that EDX also confirmed that the formed NCs are cation-rich. Using photoemission spectroscopy, see Figure 2e, S6 and S13, we observe a single contribution for the Hg 4f state. The binding energy of the Hg $4f_{7/2}$ is determined to be 100.3 eV which is consistent with the +II redox state of Hg. Within the photoemission resolution, we can thus exclude the presence of metallic Hg in the final material.

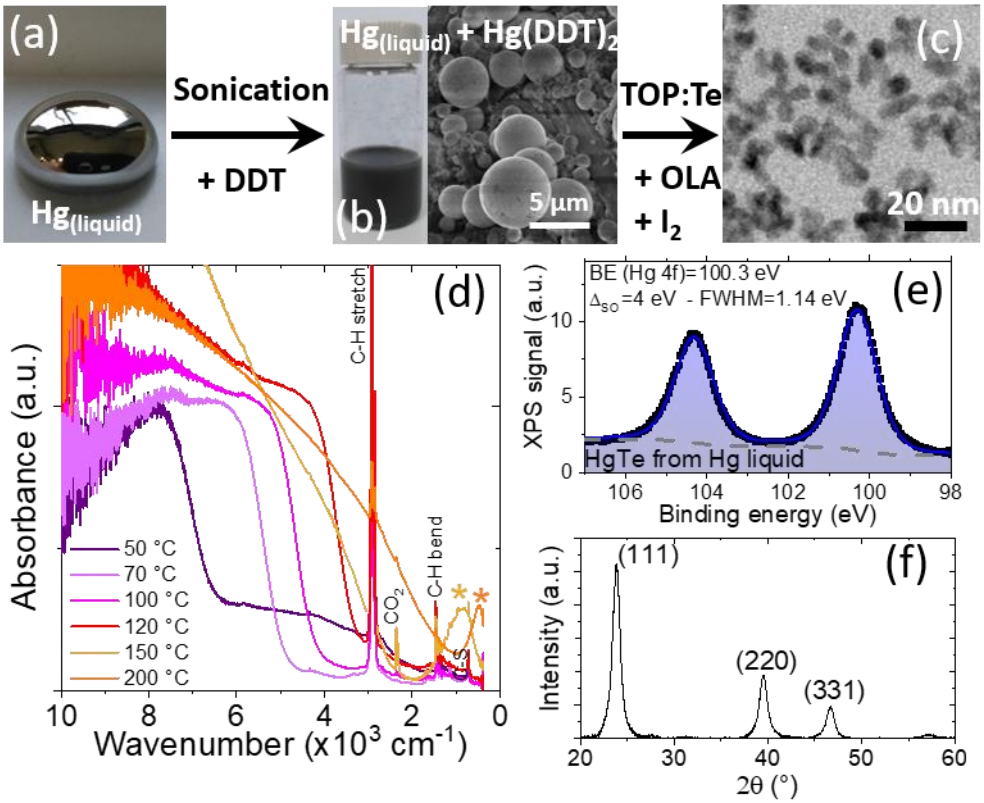

Figure 2 (a) Image of a liquid Hg drop. (b) Optical and SEM pictures of the solution of mercury dodecylthiolate prepared from liquid Hg. (c) TEM picture of HgTe QDs synthesized using liquid

*Hg as precursor. (d) Absorbance spectra of HgTe QDs synthesized from 50 °C to 200 °C using liquid Hg as precursor. * is here to highlight the intraband contribution of the absorption spectrum. (e) X-ray photoemission signal, relative to the Hg 4f state, obtained from a film made of HgTe NCs and for which the Hg precursor is liquid Hg. (f) X-ray diffraction pattern obtained from a film made of HgTe NCs and for which the Hg precursor is liquid Hg. The diffractogram is consistent with the zinc blende phase of HgTe.*

A second key advantage of this approach based on liquid mercury is the possibility to conduct highly concentrated syntheses leading to several grams of NCs per experiment.[38] A significant effort has been conducted to achieve gram scale synthesis for PbS[26,39–41], but this effort is still lacking for HgTe which has been identified as a major limitation toward industrial transfer of mid-IR NCs.[42] Here, we have been able to develop a procedure which allows the synthesis of 7 g of HgTe NCs out of 100 mL of reaction medium and which used only 50 mL of solvent for two steps of cleaning, see Figure 3a, b and Figure S15. The obtained material, observed by TEM presents similar shape and absorption features as the material synthesized with a reduced quantity of precursors, see Figure 3c. The final concentration of NCs in the reaction medium is around 100 $g.L^{-1}$, which is by far the largest value reported for HgTe, see Figure 3d.

It has been previously discussed by Livache *et al*,[42] that the introduction of a 1 cm^2 large infrared sensor in every car sold in Europe (20 millions/year) will require the synthesis of 50 kg of HgTe nanocrystals. Such amount also includes 90% of waste (from spin coating) at the fabrication steps. Previous HgTe nanocrystal methods were incompatible with mass scale production leading to such amounts. Here we have been able to obtain 7 g from less than 100 mL of reaction medium. If we assume that an operator works around 200 days/year, a simple benchtop setup can already lead to 1.4 kg/year. In SME companies, the use of large glass reactor is now well established. The amount of 50 kg can potentially be fully produced from a single 30 L reactor.

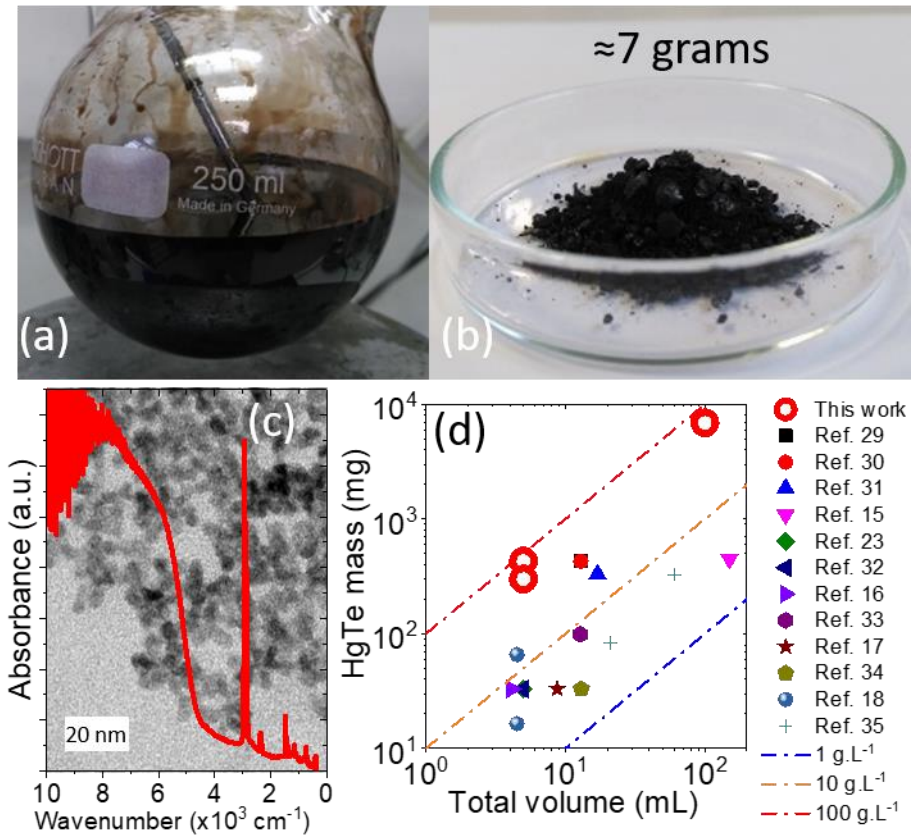

Figure 3 (a) Result of a 100 mL synthesis made from liquid Hg and leading to a highly concentrated solution of HgTe NCs. (b) Dried powder of 6.9 g HgTe QDs obtained with 100 mL of synthesis solvent. (c) Absorption spectrum of the HgTe NCs obtained after the synthesis described in part (a) and (b). The picture in the back is a TEM image of the obtained HgTe NCs. (d) Comparison of mass yield from this work to previous studies assuming a total conversion of the limiting reagent to a HgTe material from references [43–45,21,28,46,22,47,23,48,24,37].

The developed strategy based on Hg thiolate and *in situ* formed Hg thiolate is not limited to HgTe and can be extended to other chalcogenides (*i.e.* HgS and HgSe), see Figure 4b and c. As for previously reported syntheses, the spectrum of HgS[29] and HgSe[31,49] presents an intraband feature in the mid-infrared, see Figure 4a, S16 and S17. It is worth noting that the chalcogenide precursors cannot be TOP:S and TOP:Se and we rather use $(NH_4)_2S$ and Se in oleylamine and DDT respectively for the synthesis of HgS and HgSe.

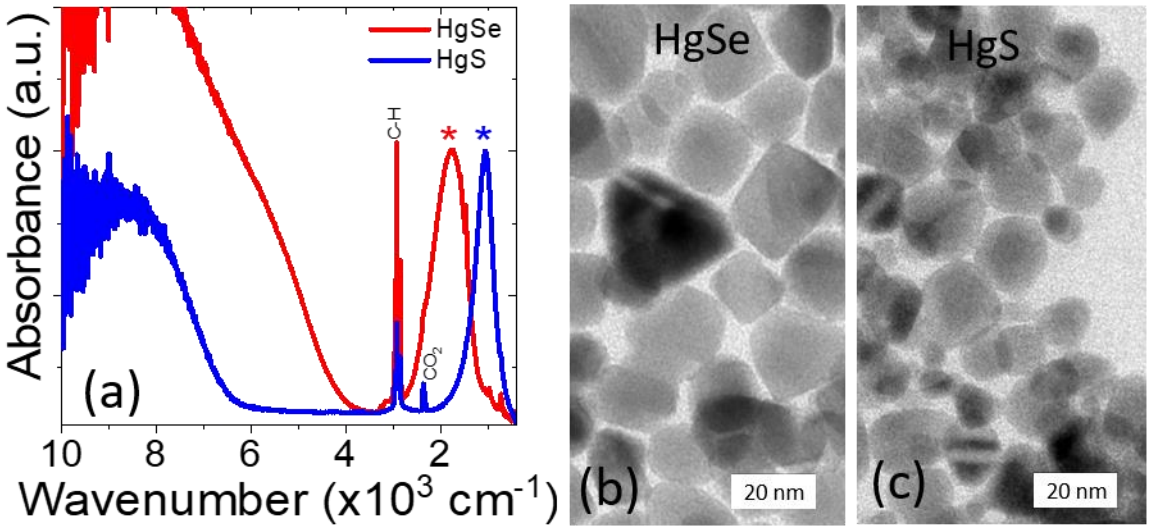

*Figure 4 (a) Absorbance spectra of HgSe (red) and HgS (blue) QDs synthesized with mercury dodecylthiolate. * is here to highlight the intraband contribution of the absorption spectrum. TEM pictures of (b) HgSe and (c) HgS QDs. Data relative to synthesis with liquid Hg are reported in S16 and S17.*

To demonstrate the potential of this new material for optoelectronic applications, we probed their transport properties in a field effect transistor.[50] We used an ion gel electrolyte configuration, see Figure S18 for a scheme of the setup.[51] The large capacitance of the electrolyte allows to broadly tune the relative position of the Fermi level with respect to the band over several hundred of meV, which is similar to the band gap value of this material. As a result, it is possible to achieve both hole and electron injection in this material. Consequently, all material appears ambipolar, we nevertheless observe a clear change in the ratio of hole vs electron conduction with the growth method.

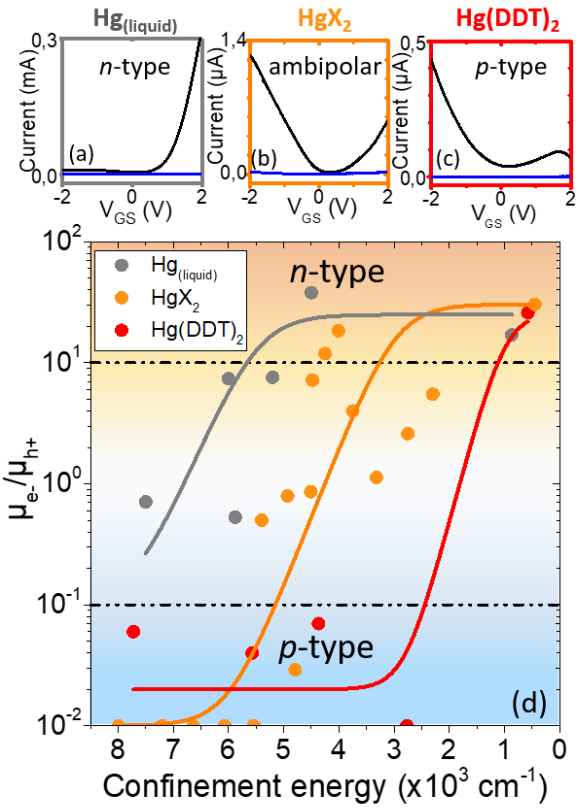

Figure 5 Transfer curves of HgTe QDs with excitonic feature around 4000 cm^{-1} synthesized with liquid mercury (a), mercury halogenide (b) and mercury dodecylthiolate (c) with drain-source current (black) and gate-source current (blue). (d) Mobility ratio of electrons and holes for HgTe QDs synthesized using the three different mercury precursors and with different confinement energies (ie taken equal to the interband transition energies).

It was previously demonstrated[8] that HgTe NCs show a transition from p-type to n-type as size (and confinement) gets increased (respectively reduced). We have measured the transfer curves of HgTe NCs based transistors with various sizes for the three types of synthesis based on: (i) $HgCl_2$, (*ii*) Hg thiolate and (*iii*) liquid Hg, see Figure S19-S21. They do present, as expected, a transition of the conduction from p to n-type as the NC size is increased, see Figure 5d. Note that such transition is also consistent with the appearing of the intraband contribution in the infrared spectrum of the largest nanoparticle which indicate a stronger doping magnitude.

However, the threshold of this transition varies from synthesis to synthesis. For a given size, the synthesis based on liquid Hg tends to be more n-type, while the one based on thiolate is more p-type, see Figure 5a-c. Because we observe from photoemission no trace of Hg^0, we can exclude that the change of doping is the result of a change of the Hg redox state. Alternatively, we can speculate that each growth condition affects the facet which are the most present on the nanocrystal surface. This leads to small modification of the surface Hg excess and finally tune the doping.

In the last part of the paper we discuss the use of this material (HgTe prepared from liquid Hg) for infrared sensing. We synthetize particle with a band gap at 4900 cm^{-1} (600 meV) corresponding to an absorption the extended short-wave infrared, see Figure 6a. Once the material is processed under thin and the ligand exchange for

ethanedithiol (EDT) the band edge energy remains almost unchanged but the feature gets broader. Transport in HgTe nanoparticles connected to gold electrodes appears to be ohmic, see Figure 6b. More striking is the temperature dependence of the material, which presents a large decay of the film conductance upon cooling, see the inset of Figure 6b. An Arrhenius fit of the current leads to an activation energy of 226 meV. This is quite close to half the value of the optical band gap (600/2=300 meV) which suggests a quasi-intrinsic nature for the semiconductor. It is also worth pointing that this value is also much larger than the one obtained for HgTe nanoparticles resulting from the mercury halide precursor. In the latter case, the activation energy is 150 meV for a band gap of 720 meV[52] (6000 cm^{-1}) or 114 meV for a band gap of 500 meV[53] (4000 cm^{-1}). Last the time response of the sample has been tested under illumination by a 1.55 µm laser diode, see Figure 6c. Turn on time has been estimated to be 21 µs. For the decay time, we observe two components a fast one around 3µs and a longer one at 153 µs. All characteristic time remains compatible with fast imaging.

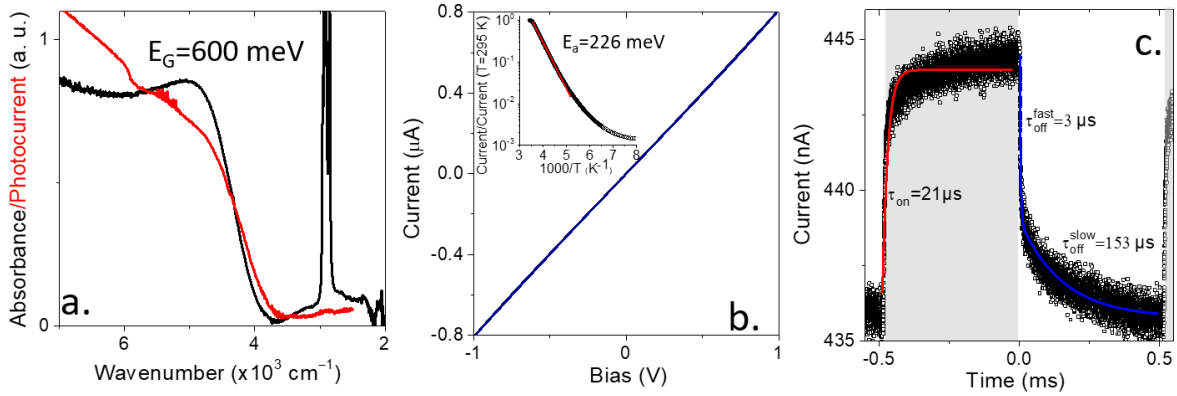

Figure 6a. absorption and photocurrent spectra of HgTe nanocrystals obtained from liquid Hg synthesis. b. I-V curve from a thin film of HgTe nanocrystals obtained from liquid Hg synthesis after EDT ligand exchange. The inset provide the temperature dependence of the current for thin film of HgTe nanocrystals obtained from liquid Hg synthesis. The red curve is an arrhenius'fit of the data revealing an activation energy of 226 meV. c. Current as a function of time for a thin film of HgTe nanocrystals obtained from liquid Hg synthesis under illumination by a 1.55 µm laser turning on and off. The laser in on state corresponds to the grey part of the graph.

CONCLUSIONS

We propose a new synthetic strategy for the synthesis of mercury chalcogenides NCs. The method relies on the use of Hg thiolate as the Hg source. We demonstrate that the Hg thiolate can be prepared *in situ* from liquid mercury. This approach can be used to obtain highly concentrated NCs solutions (≈100 $g.L^{-1}$). Significant amount (7 g) of infrared NCs can be obtained from extremely reduced reaction volume. Compared to conventional HgTe synthesis, the method reduces exposition of workforce to hydrophilic mercury species and drastically decreases the solvent consumption. The procedure can be extended to HgS and HgSe. The transport properties of the obtained HgTe have been tested in a transistor configuration and we observe a transition from p to n-type with size. The size threshold is strongly dependent on the way the NCs are

grown. This is promising for the design of p-n photodiodes with enhanced photocharges dissociation. Another promising direction will relate to the use of amalgam. Many noble metal can be mixed in liquid Hg,[54] this approach may be use to further control the doping of the nanoparticle though the introduction of impurities with redox state different from +II. Last, we have tested the potential of this material for IR sensing and demonstrate similar performances to previously reported synthesis.

ASSOCIATED CONTENT

Supporting Information

The Supporting Information is available free of charge on the ACS Publications website.

Supporting information include chemical and details about material characterization, as well as methods for precursors and nanocrystal synthesis. Additional data relative to electronic transport are also provided (PDF).

AUTHOR INFORMATION

Corresponding Author

nicolas.goubet@sorbonne-universite.fr and el@insp.upmc.fr

ACKNOWLEDGMENT

EL acknowledges the financial support of the European Research Council (ERC) starting grant (blackQD – n°756225). We thank Agence Nationale de la Recherche for funding through grant IPER-nano2, Copin, Graskop and Frontal. This work was supported by French state funds managed by the ANR within the Investissements d'Avenir programme under reference ANR-11-IDEX-0004-02, and more specifically within the framework of the Cluster of Excellence MATISSE. We acknowledge the use of clean-room facilities from the “Centrale de Proximité Paris-Centre”. This work has been supported by the Region Ile-de-France in the framework of DIM Nano-K. JQ thanks Chinese Scholar Council for PhD. funding. AC thanks Agence Innovation Defense for PhD funding.

REFERENCES

(1) Goubet, N.; Jagtap, A.; Livache, C.; Martinez, B.; Portalès, H.; Xu, X. Z.; Lobo, R. P. S. M.; Dubertret, B.; Lhuillier, E. Terahertz HgTe Nanocrystals: Beyond Confinement. *J. Am. Chem. Soc.* **2018**, *140*, 5033–5036.

(2) Shirasaki, Y.; Supran, G. J.; Bawendi, M. G.; Bulović, V. Emergence of Colloidal Quantum-Dot Light-Emitting Technologies. *Nat. Photonics* **2013**, *7*, 13–23.

(3) Lu, H.; Carroll, G. M.; Neale, N. R.; Beard, M. C. Infrared Quantum Dots: Progress, Challenges, and Opportunities. *ACS Nano* **2019**, *13*, 939–953.

(4) Lu, K.; Wang, Y.; Liu, Z.; Han, L.; Shi, G.; Fang, H.; Chen, J.; Ye, X.; Chen, S.; Yang, F.; et al. High-Efficiency PbS Quantum-Dot Solar Cells with Greatly Simplified Fabrication Processing via “Solvent-Curing.” *Adv. Mater.* **2018**, *30*, 1707572.

(5) *Colloidal Quantum Dot Optoelectronics and Photovoltaics*, 1 edition.; Konstantatos, G., Sargent, E. H., Eds.; Cambridge University Press: New York, 2013.
(6) Ramade, J.; Qu, J.; Chu, A.; Greboval, C.; Livache, C.; Goubet, N.; Martinez, B.; Vincent, G.; Lhuillier, E. Potential of Colloidal Quantum Dot Based Solar Cell for Near-Infrared Active Detection. *ACS Photonics* **2020**, *7*, 272-278.
(7) Tang, X.; Ackerman, M. M.; Chen, M.; Guyot-Sionnest, P. Dual-Band Infrared Imaging Using Stacked Colloidal Quantum Dot Photodiodes. *Nat. Photonics* **2019**, *13*, 277-282.
(8) Jagtap, A.; Martinez, B.; Goubet, N.; Chu, A.; Livache, C.; Gréboval, C.; Ramade, J.; Amelot, D.; Trousset, P.; Triboulin, A.; et al. Design of a Unipolar Barrier for a Nanocrystal-Based Short-Wave Infrared Photodiode. *ACS Photonics* **2018**, *5*, 4569–4576.
(9) Tang, X.; Tang, X.; Lai, K. W. C. Scalable Fabrication of Infrared Detectors with Multispectral Photoresponse Based on Patterned Colloidal Quantum Dot Films. *ACS Photonics* **2016**, *3*, 2396–2404.
(10) Pietryga, J. M.; Schaller, R. D.; Werder, D.; Stewart, M. H.; Klimov, V. I.; Hollingsworth, J. A. Pushing the Band Gap Envelope: Mid-Infrared Emitting Colloidal PbSe Quantum Dots. *J. Am. Chem. Soc.* **2004**, *126*, 11752–11753.
(11) Weidman, M. C.; Beck, M. E.; Hoffman, R. S.; Prins, F.; Tisdale, W. A. Monodisperse, Air-Stable PbS Nanocrystals via Precursor Stoichiometry Control. *ACS Nano* **2014**, *8*, 6363–6371.
(12) Chen, M.; Lu, H.; Abdelazim, N. M.; Zhu, Y.; Wang, Z.; Ren, W.; Kershaw, S. V.; Rogach, A. L.; Zhao, N. Mercury Telluride Quantum Dot Based Phototransistor Enabling High-Sensitivity Room-Temperature Photodetection at 2000 Nm. *ACS Nano* **2017**, *11*, 5614–5622.
(13) Rauch, T.; Böberl, M.; Tedde, S. F.; Fürst, J.; Kovalenko, M. V.; Hesser, G.; Lemmer, U.; Heiss, W.; Hayden, O. Near-Infrared Imaging with Quantum-Dot-Sensitized Organic Photodiodes. *Nat. Photonics* **2009**, *3*, 332–336.
(14) Keuleyan, S.; Lhuillier, E.; Brajuskovic, V.; Guyot-Sionnest, P. Mid-Infrared HgTe Colloidal Quantum Dot Photodetectors. *Nat. Photonics* **2011**, *5*, 489–493.
(15) Ackerman, M. M.; Tang, X.; Guyot-Sionnest, P. Fast and Sensitive Colloidal Quantum Dot Mid-Wave Infrared Photodetectors. *ACS Nano* **2018**, *12*, 7264–7271.
(16) Abdelazim, N. M.; Zhu, Q.; Xiong, Y.; Zhu, Y.; Chen, M.; Zhao, N.; Kershaw, S. V.; Rogach, A. L. Room Temperature Synthesis of HgTe Quantum Dots in an Aprotic Solvent Realizing High Photoluminescence Quantum Yields in the Infrared. *Chem. Mater.* **2017**, *29*, 7859–7867.
(17) Sergeev, A. A.; Pavlov, D. V.; Kuchmizhak, A. A.; Lapine, M. V.; Yiu, W. K.; Dong, Y.; Ke, N.; Juodkazis, S.; Zhao, N.; Kershaw, S. V.; et al. Tailoring Spontaneous Infrared Emission of HgTe Quantum Dots with Laser-Printed Plasmonic Arrays. *Light Sci. Appl.* **2020**, *9*, 1–10.
(18) Geiregat, P.; Houtepen, A. J.; Sagar, L. K.; Infante, I.; Zapata, F.; Grigel, V.; Allan, G.; Delerue, C.; Thourhout, D. V.; Hens, Z. Continuous-Wave Infrared Optical Gain and Amplified Spontaneous Emission at Ultralow Threshold by Colloidal HgTe Quantum Dots. *Nat. Mater.* **2018**, *17*, 35-42.
(19) Kershaw, S. V.; Susha, A. S.; Rogach, A. L. Narrow Bandgap Colloidal Metal Chalcogenide Quantum Dots: Synthetic Methods, Heterostructures, Assemblies, Electronic and Infrared Optical Properties. *Chem. Soc. Rev.* **2013**, *42*, 3033–3087.

(20) Green, M.; Mirzai, H. Synthetic Routes to Mercury Chalcogenide Quantum Dots. *J. Mater. Chem. C* **2018**, *6*, 5097–5112.
(21) Kovalenko, M. V.; Kaufmann, E.; Pachinger, D.; Roither, J.; Huber, M.; Stangl, J.; Hesser, G.; Schäffler, F.; Heiss, W. Colloidal HgTe Nanocrystals with Widely Tunable Narrow Band Gap Energies: From Telecommunications to Molecular Vibrations. *J. Am. Chem. Soc.* **2006**, *128*, 3516–3517.
(22) Keuleyan, S.; Lhuillier, E.; Guyot-Sionnest, P. Synthesis of Colloidal HgTe Quantum Dots for Narrow Mid-IR Emission and Detection. *J. Am. Chem. Soc.* **2011**, *133*, 16422–16424.
(23) Keuleyan, S. E.; Guyot-Sionnest, P.; Delerue, C.; Allan, G. Mercury Telluride Colloidal Quantum Dots: Electronic Structure, Size-Dependent Spectra, and Photocurrent Detection up to 12 Mm. *ACS Nano* **2014**, *8*, 8676–8682.
(24) Shen, G.; Chen, M.; Guyot-Sionnest, P. Synthesis of Nonaggregating HgTe Colloidal Quantum Dots and the Emergence of Air-Stable n-Doping. *J. Phys. Chem. Lett.* **2017**, *8* 2224–2228.
(25) Jean, J.; Xiao, J.; Nick, R.; Moody, N.; Nasilowski, M.; Bawendi, M.; Bulović, V. Synthesis Cost Dictates the Commercial Viability of Lead Sulfide and Perovskite Quantum Dot Photovoltaics. *Energy Environ. Sci.* **2018**, *11*, 2295–2305.
(26) Yarema, M.; Yarema, O.; Lin, W. M. M.; Volk, S.; Yazdani, N.; Bozyigit, D.; Wood, V. Upscaling Colloidal Nanocrystal Hot-Injection Syntheses via Reactor Underpressure. *Chem. Mater.* **2017**, *29*, 796–803.
(27) Busupalli, B.; Kummara, S.; Kumaraswamy, G.; Prasad, B. L. V. Ultrathin Sheets of Metal or Metal Sulfide from Molecularly Thin Sheets of Metal Thiolates in Solution. *Chem. Mater.* **2014**, *26*, 3436–3442.
(28) Kim, S.; Kim, T.; Im, S. H.; Seok, S. I.; Kim, K. W.; Kim, S.; Kim, S.-W. Bandgap Engineered Monodisperse and Stable Mercury Telluride Quantum Dots and Their Application for Near-Infrared Photodetection. *J. Mater. Chem.* **2011**, *21*, 15232–15236.
(29) Jeong, K. S.; Deng, Z.; Keuleyan, S.; Liu, H.; Guyot-Sionnest, P. Air-Stable n-Doped Colloidal HgS Quantum Dots. *J. Phys. Chem. Lett.* **2014**, *5*, 1139–1143.
(30) Robin, A.; Livache, C.; Ithurria, S.; Lacaze, E.; Dubertret, B.; Lhuillier, E. Surface Control of Doping in Self-Doped Nanocrystals. *ACS Appl. Mater. Interfaces* **2016**, *8*, 27122–27128.
(31) Lhuillier, E.; Scarafagio, M.; Hease, P.; Nadal, B.; Aubin, H.; Xu, X. Z.; Lequeux, N.; Patriarche, G.; Ithurria, S.; Dubertret, B. Infrared Photodetection Based on Colloidal Quantum-Dot Films with High Mobility and Optical Absorption up to THz. *Nano Lett.* **2016**, *16*, 1282–1286.
(32) Izquierdo, E.; Robin, A.; Keuleyan, S.; Lequeux, N.; Lhuillier, E.; Ithurria, S. Strongly Confined HgTe 2D Nanoplatelets as Narrow Near-Infrared Emitters. *J. Am. Chem. Soc.* **2016**, *138*, 10496–10501.
(33) Rinnerbauer, V.; Hingerl, K.; Kovalenko, M.; Heiss, W. Effect of Quantum Confinement on Higher Transitions in HgTe Nanocrystals. *Appl. Phys. Lett.* **2006**, *89*, 193114.
(34) Daeneke, T.; Khoshmanesh, K.; Mahmood, N.; Castro, I. A. de; Esrafilzadeh, D.; Barrow, S. J.; Dickey, M. D.; Kalantar-zadeh, K. Liquid Metals: Fundamentals and Applications in Chemistry. *Chem. Soc. Rev.* **2018**, *47*, 4073–4111.
(35) Pokroy, B.; Aichmayer, B.; Schenk, A. S.; Haimov, B.; Kang, S. H.; Fratzl, P.; Aizenberg, J. Sonication-Assisted Synthesis of Large, High-Quality Mercury Thiolate Single Crystals Directly from Liquid Mercury. *J. Am. Chem. Soc.* **2010**, *132*, 14355–14357.

(36) Ramesh, G. V.; Prasad, M. D.; Radhakrishnan, T. P. Mercury Nanodrops and Nanocrystals. *Chem. Mater.* **2011**, *23*, 5231–5236.
(37) Hudson, M. H.; Chen, M.; Kamysbayev, V.; Janke, E. M.; Lan, X.; Allan, G.; Delerue, C.; Lee, B.; Guyot-Sionnest, P.; Talapin, D. V. Conduction Band Fine Structure in Colloidal HgTe Quantum Dots. *ACS Nano* **2018**, *12*, 9397–9404.
(38) Williamson, C. B.; Nevers, D. R.; Hanrath, T.; Robinson, R. D. Prodigious Effects of Concentration Intensification on Nanoparticle Synthesis: A High-Quality, Scalable Approach. *J. Am. Chem. Soc.* **2015**, *137*, 15843–15851.
(39) Cademartiri, L.; Bertolotti, J.; Sapienza, R.; Wiersma, D. S.; von Freymann, G.; Ozin, G. A. Multigram Scale, Solventless, and Diffusion-Controlled Route to Highly Monodisperse PbS Nanocrystals. *J. Phys. Chem. B* **2006**, *110*, 671–673.
(40) Bera, A.; Busupalli, B.; Prasad, B. L. V. Solvent-Less Solid State Synthesis of Dispersible Metal and Semiconducting Metal Sulfide Nanocrystals. *ACS Sustain. Chem. Eng.* **2018**, *6*, 12006–12016.
(41) Hendricks, M. P.; Campos, M. P.; Cleveland, G. T.; Plante, I. J.-L.; Owen, J. S. A Tunable Library of Substituted Thiourea Precursors to Metal Sulfide Nanocrystals. *Science* **2015**, *348*, 1226–1230.
(42) Livache, C.; Martinez, B.; Goubet, N.; Ramade, J.; Lhuillier, E. Road Map for Nanocrystal Based Infrared Photodetectors. *Front. Chem.* **2018**, *6,* 575.
(43) Green, M.; Wakefield, G.; Dobson, P. J. A Simple Metalorganic Route to Organically Passivated Mercury Telluride Nanocrystals. *J. Mater. Chem.* **2003**, *13*, 1076–1078.
(44) Li, L. S.; Wang, H.; Liu, Y.; Lou, S.; Wang, Y.; Du, Z. Room Temperature Synthesis of HgTe Nanocrystals. *J. Colloid Interface Sci.* **2007**, *308*, 254–257.
(45) Piepenbrock, M.-O. M.; Stirner, T.; Kelly, S. M.; O'Neill, M. A Low-Temperature Synthesis for Organically Soluble HgTe Nanocrystals Exhibiting Near-Infrared Photoluminescence and Quantum Confinement. *J. Am. Chem. Soc.* **2006**, *128*, 7087–7090.
(46) Im, S. H.; Kim, H.; Kim, S. W.; Kim, S.-W.; Seok, S. I. Efficient HgTe Colloidal Quantum Dot-Sensitized near-Infrared Photovoltaic Cells. *Nanoscale* **2012**, *4*, 1581–1584.
(47) Keuleyan, S.; Kohler, J.; Guyot-Sionnest, P. Photoluminescence of Mid-Infrared HgTe Colloidal Quantum Dots. *J. Phys. Chem. C* **2014**, *118*, 2749–2753.
(48) Nengjie, H.; Shuchi, G.; Gerasimos, K. MoS_2–HgTe Quantum Dot Hybrid Photodetectors beyond 2 Mm. *Adv. Mater.* **2017**, *29*, 1606576.
(49) Deng, Z.; Jeong, K. S.; Guyot-Sionnest, P. Colloidal Quantum Dots Intraband Photodetectors. *ACS Nano* **2014**, *8*, 11707–11714.
(50) Lhuillier, E.; Keuleyan, S.; Zolotavin, P.; Guyot-Sionnest, P. Mid-Infrared HgTe/As2S3 Field Effect Transistors and Photodetectors. *Adv. Mater.* **2013**, *25*, 137–141.
(51) Lhuillier, E.; Ithurria, S.; Descamps-Mandine, A.; Douillard, T.; Castaing, R.; Xu, X. Z.; Taberna, P.-L.; Simon, P.; Aubin, H.; Dubertret, B. Investigating the N- and p-Type Electrolytic Charging of Colloidal Nanoplatelets. *J. Phys. Chem. C* **2015**, *119*, 21795–21799.
(52) Chu, A.; Martinez, B.; Ferré, S.; Noguier, V.; Gréboval, C.; Livache, C.; Qu, J.; Prado, Y.; Casaretto, N.; Goubet, N.; et al. HgTe Nanocrystals for SWIR Detection and Their Integration up to the Focal Plane Array. *ACS Appl. Mater. Interfaces* **2019**, *11*, 33116–33123.
(53) Jagtap, A.; Goubet, N.; Livache, C.; Chu, A.; Martinez, B.; Gréboval, C.; Qu, J.; Dandeu, E.; Becerra, L.; Witkowski, N.; et al. Short Wave Infrared Devices Based

on HgTe Nanocrystals with Air Stable Performances. *J. Phys. Chem. C* **2018**, *122*, 14979–14985.

(54) Mertens, S. F. L.; Gara, M.; Sologubenko, A. S.; Mayer, J.; Szidat, S.; Krämer, K. W.; Jacob, T.; Schiffrin, D. J.; Wandlowski, T. Au@Hg Nanoalloy Formation Through Direct Amalgamation: Structural, Spectroscopic, and Computational Evidence for Slow Nanoscale Diffusion. *Adv. Funct. Mater.* **2011**, *21*, 3259–3267.

TOC graphic

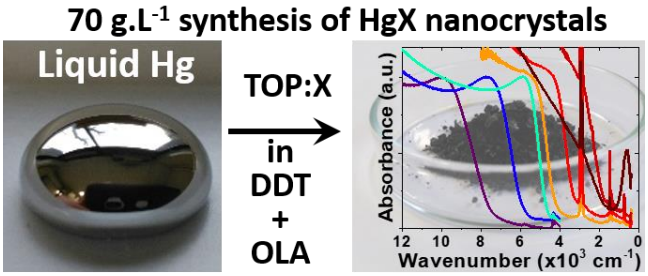
70 g.L-1 synthesis of HgX nanocrystals
Liquid Hg
TOP:X
in
DDT
+
OLA
Absorbance (a.u.)
12 10 8 6 4 2 0
Wavenumber (x10³ cm⁻¹)